International Journal of Hydrogen Energy 136 (2025) 1073–1085

Contents lists available at ScienceDirect

International Journal of Hydrogen Energy

journal homepage: www.elsevier.com/locate/he

Different architectures of thin film bilayers based on TiO_2 and CuO for green hydrogen generation

Joanna Banaś-Gac [a,*], Marta Radecka [b], Eduard Llobet [c], Ewa Partyka-Jankowska [d], Katarzyna Zakrzewska [a]

[a] Faculty of Computer Science, Electronics and Telecommunications, AGH University of Krakow, Krakow, Poland
[b] Faculty of Materials Science and Ceramics, AGH University of Krakow, Krakow, Poland
[c] Department of Electronic, Electrical and Automatic Engineering, Rovira i Virgili University, Tarragona, Spain
[d] SOLARIS National Synchrotron Radiation Centre, Jagiellonian University, Krakow, Poland

ARTICLE INFO

Handling Editor: Ibrahim Dincer

Keywords:
Green hydrogen generation
Photoelectrochemical water splitting
Thin film bilayers
Heterojunctions TiO_2/CuO

ABSTRACT

Green hydrogen becomes one of the most important of all other forms due to ecological issues, described in directives requiring the transformation to energy sources with the lowest possible carbon footprint. The application of the PhotoElectrochemical Cell where hydrogen is produced with the direct use of solar energy is the best solution. Bilayer and multilayered systems based on CuO, especially in combination with TiO_2 seem to be the most frequently studied of all heterostructured nanomaterials when considering green hydrogen generation. The interface created between rough surface of CuO and smooth TiO_2 surface ensures the highest photocurrent when the top layer is of about 150 nm. For CuO(top)/TiO_2 heterojunction characterized by rough/rough interface, photoeletrochemical performance also improves with increasing thickness of the top layer up to 100 nm. The cathodic character of the photocurrent is observed for both TiO_2(top)/CuO and CuO(top)/TiO_2 bilayers.

1. Introduction

Intense efforts, concerning transformation of the power sector towards emission-free, decarbonized and renewable ways of energy production, storage, transfer and usage, focus, in the first place, on hydrogen as a new, efficient energy carrier. Numerous, excellent publications devoted to this topic have appeared only recently [1–5]. Classification of the hydrogen sources based on the color scheme extending from brown to green has been proposed [6]. It is well-known that green color assigned symbolically to hydrogen means that this type of power generation is the most ecologically friendly and pollutant-free thus requires extensive scientific research. However, in practice, majority of hydrogen production methods are based on coal gasification or steam methane reforming being referred to as brown and gray, respectively. If the by-products such as CO_2 are captured and stored, we deal with blue hydrogen. Green hydrogen can be generated by water splitting in the process of electro- or photolysis. Electrolysis of water supported by solar cells or windmills as electricity supplies is considered to belong to the same category of green hydrogen sources. Recently, one can follow a profound discussion on the hydrogen colors and particularly on the most suitable factors on which such classification should be based. According to Kusoglu [7], traditional color coding employs mixed categories: pathways (processes), sources (electricity or fuels) level of CO_2 emission, thus and seems to be insufficient. Emerging new methods of hydrogen generation such as biomass pathways escape from this classification. Moreover, a new trend can be observed recently to incorporate life cycle analysis LCA, i.e., a comprehensive evaluation of the environmental, social and economic aspects, from the production to final use of green hydrogen [4]. Therefore, more work is needed to encompass these new challenges especially in the field of nanomaterials and thin films for green hydrogen generation by water photolysis.

It seems that, the application of the PhotoElectrochemical Cell (PEC) where hydrogen is produced with the direct use of solar energy is the best solution to the problem. In terms of efficiency of hydrogen generation, one of the most important challenges to be faced is the dynamics of the processes taking place in the cell. The key issue is to match the lifetime of photogenerated carriers to the time needed for the reaction of water splitting to occur. Therefore, it is necessary to conduct research on

This article is part of a special issue entitled: ANM2024 (Titus) published in International Journal of Hydrogen Energy.

* Corresponding author.
E-mail address: jbanas@agh.edu.pl (J. Banaś-Gac).

https://doi.org/10.1016/j.ijhydene.2025.03.036
Received 20 December 2024; Received in revised form 13 February 2025; Accepted 3 March 2025
Available online 10 March 2025

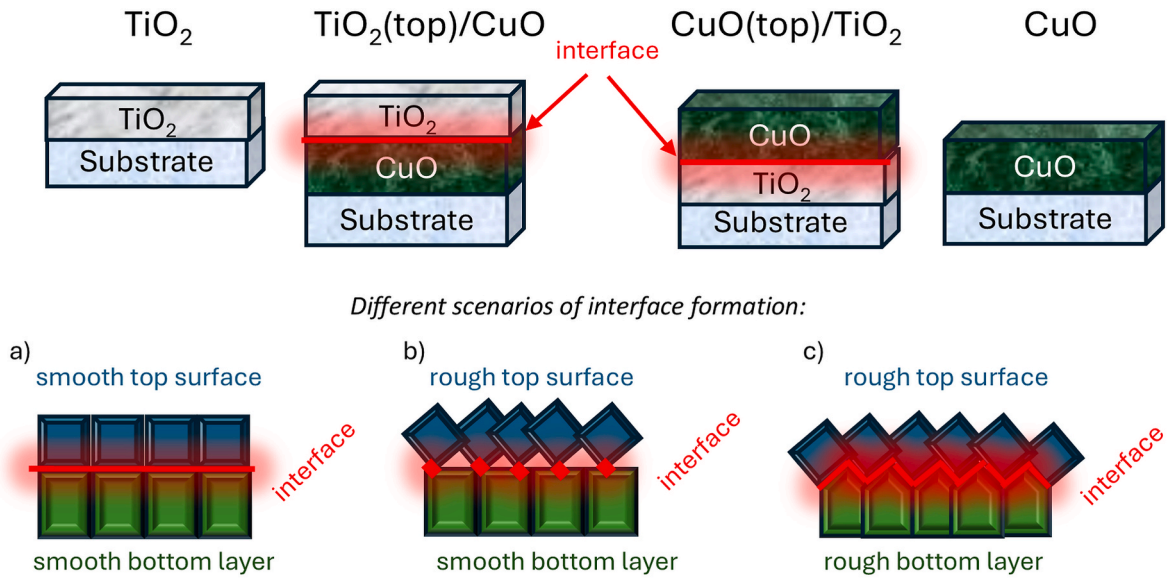

Fig. 1. Graphical schemes of single and bilayer thin films deposited by rf magnetron sputtering. Different scenarios of interface formation depending on the smooth and rough morphology of thin films: both smooth layers (a), rough top surface and smooth bottom layer (b) and both rough surfaces (c).

ensuring the most effective separation of photo-excited carriers. Multicomponent materials gain an increasing scientific interest in the photoelectrochemistry as they open up new exciting possibilities due to the synergetic effect [8]. System with a precisely planned architecture performs more favourably in comparison to a simple composite in the case of which a random distribution of individual components usually takes place. Bilayer and multilayered systems based on CuO, especially in combination with TiO_2 seem to be the most promising of all heterostructured nanomaterials when considering green hydrogen generation. Especially in the case of the above-mentioned process dynamics in the PEC cell, a bilayer heterojunction is a system in which the existence of the interface could contribute to formation of an internal electric field. Similar process of creation of the electric field in diodes, capable of efficient separation of photogenerated electron-hole pairs, results in a significant reduction of recombination of charge carriers.

Focusing on the processes taking place at the interface, it will be demonstrated in this paper that the architecture of the interface between components of heterostructures has a key impact on the operation of the complex system in green hydrogen generation. In order to examine such a system, it is worth to choose completely different semiconductors as far as band structure and morphology are concerned. Therefore, to fully highlight the influence of the connection type, semiconductors of very well-known photoelectrochemical properties [9,10] were selected for testing interface – titanium dioxide and copper oxides in the form of thin films. The main reason is that copper oxides arise as model materials to study optical properties related to roughness of thin film manifested by scattering phenomena. Differences in roughness between CuO and TiO_2 could be a game changer in the case of interface formation in heterostructure materials and thus make it possible to trace the influence of interface architecture on charge carriers transport in light induced processes. In the literature, there are several examples of heterostructures based on copper oxides only and in connection with titanium dioxide. Wang et al. proposed electrodeposited Cu_2O which conductivity type is adjusted from p-type to n-type through annealing process and thus enables the creation of p-n junction [11]. This idea allows to obtain PEC system composed of one chemical compound Cu_2O as a photocathode and photoanode. Alotaibi et al. described CuO–Cu_2O heterojunction in which the separation of photogenerated charge carriers is triggered by obtaining a greater specific surface area [12]. Authors claimed that the enhancement in PEC performance is mainly related to morphological aspect and surface defects. Zhang et al. investigated CuO/Cu_2O/Cu junction dedicated as a photocathode for water splitting through optimization of Cu_2O crystal orientation and CuO as a layer protective against photocorrosion of Cu_2O [13]. Similar junction was proposed by Wang et al. [14]. CuO/TiO_2/Cu_2O/Cu, system enriched with TiO_2 was characterized by suppressed electron transfer at the semiconductor-electrolyte interface and promoted electron transfer between Cu_2O to CuO [14]. TiO_2(top)/CuO system obtained by means of magnetron sputtering for photocatalytic degradation of organic wastes was described by Hao et al. [15]. The authors proved the influence of the thickness of both layers on the functional properties. The improvement in the photocatalytic performance was assigned to the optimized porosity and enlarged specific surface area, which result in an increased number of sites reactive during the chemical reactions. Moreover, suitable TiO_2 thickness has a positive effect on the efficiency of charge carrier separation process. Interesting phenomenon of light-driven photoelectrochemical switching was described by Long et al. [16] based on the wavelength-controlled change in the photocurrent direction for a p-n hybrid junction. The authors concluded that switching effect is observed when the valence band (VB) and conduction band (CB) edges of an n-type constituent are more positive than for a p-type. Other aspects which have an impact on the photoelectrochemical response are the applied potential and presence of electron and hole scavengers.

In this work the problem of the effect of the architecture of the TiO_2/CuO based heterojunctions suitable for photoelectrochemical applications will be addressed also from the morphological point of view. Fig. 1 presents a scheme of TiO_2 and CuO thin films as well as TiO_2(top)/CuO and CuO(top)/TiO_2bilayers. The physical features and surface morphology of both components influence the nature of the interface of the resulting heterostructures. Fig. 1a–c shows different scenarios of interface formation based on surface properties of both components of the formed junction. Fig. 1a presents the interface constructed by covering a smooth bottom layer with the smooth top surface. As obtained interface is perfectly flat and thus the layers adhere perfectly to each other. Fig. 1b shows the interface between the smooth bottom layer and the rough upper surface, which is discontinuous and consists of single contact points between both layers. The last type of interface is created by applying a rough layer to a rough substrate (Fig. 1c), the interface has an irregular shape but connects both layers tightly. The novelty of this work is that the discussion of functional properties of the bilayer composed of TiO_2 and CuO includes both the configuration with TiO_2 on top i.e., TiO_2(top)/CuO and the reverse CuO(top)/TiO_2. In the

Table 1
TiO_2 and CuO based single and bilayer thin films.

Configuration	Sample name	Temperature during deposition (°C)	Thin film thickness (nm) determined from SEM		
			CuO	TiO_2	total
CuO	C20	350	20	–	20
	C96		96	–	96
	C220		220	–	220
amorphous TiO_2	a-T160	RT	–	160	160
	a-T220		–	220	220
	a-T314		–	314	314
crystallized TiO_2	c-T240	350	–	240	240
TiO_2(top)/CuO	T33_C208	RT	208	33	241
	T54_C208		208	54	262
	T73_C208		208	73	281
	T87_C208		208	87	295
	T151_C208		208	151	359
CuO(top)/TiO_2	C20_T320	350	20	320	340
	C100_T246		100	246	346

literature there are no works comparing the properties of both configurations in the form of thin films. The problem to be solved is to find the parameters that allow for the preparation of interface with a structure that favours the effective separation of charge carriers, which in turn causes improvement in the efficiency of redox reactions taking place in the PhotoElectrochemical Cell. The analysis of photoelectrochemical characteristics of the heterostructural photoelectrode based on CuO with TiO_2 in connection with band alignment diagrams of heterojunctions will be the basis for the choice of junction type and interface architecture, which leads to improvement in photoelectrochemical properties of electrodes and their stability. The mechanism of the photoelectrode performance is proposed for the first time for both types of heterostructure.

2. Materials and methods

2.1. Materials preparation

Both single CuO, TiO_2 and TiO_2(top)/CuO, CuO(top)/TiO_2 bilayer thin films were obtained by means of rf reactive magnetron sputtering from Cu and Ti metallic targets in an Ar/O_2 gas mixture. Ultra-high vacuum UHV system (*Prevac, Rogów Poland*) described in previous papers of our group [17–19] was applied in the deposition processes. Sequential deposition cycles performed without breaking a vacuum were used to obtain bilayers with a well-defined interface. Single CuO thin films, crystallized TiO_2 and CuO(top)/TiO_2 bilayers were deposited on substrates heated up to 350 °C. Amorphous TiO_2 and TiO_2(top)/CuO bilayers were sputtered at room temperature (RT). The ratio of O_2 in the reactive gas mixture $O_2/Ar + O_2$ during CuO thin film deposition was equal to 35% and for TiO_2 deposition 20%. Sputtering was performed with the use of two 2" diameter discs: titanium of purity 99.995% (Kurt J. Lesker Co.) and copper of purity 99.999% (Kurt J. Lesker Co.) with the use of radio frequency rf power supply equipped with an automatic matching network keeping reflected power equal to zero. Deposition rate of about 13 nm/min was maintained by applying fixed power densities equal to 4.4 W/cm^2 and 9.9 W/cm^2 for copper and titanium, respectively. Different substrates were used to perform all the necessary characterization [19]. Samples, which were investigated in this work, are summarized in Table 1.

2.2. Material characterization

X-ray diffraction (XRD) in Grazing Incidence configuration (GID) and X-ray reflectivity (XRR) were performed by X'Pert PRO PANalytical diffractometer equipped with a Cu lamp ($\lambda = 0.154$ nm). Synchrotron measurements were carried out in SOLARIS National Synchrotron Radiation Centre (Krakow, Poland) [20] at PIRX beamline. X-ray absorption spectra were recorded in the Total Electron Yield (TEY) mode for titanium Ti L_{23} and copper Cu L_{23} lines within the following energy ranges: 440–520 eV and 910–1040 eV, respectively. Microscopic observations were conducted with the use of Scanning Electron

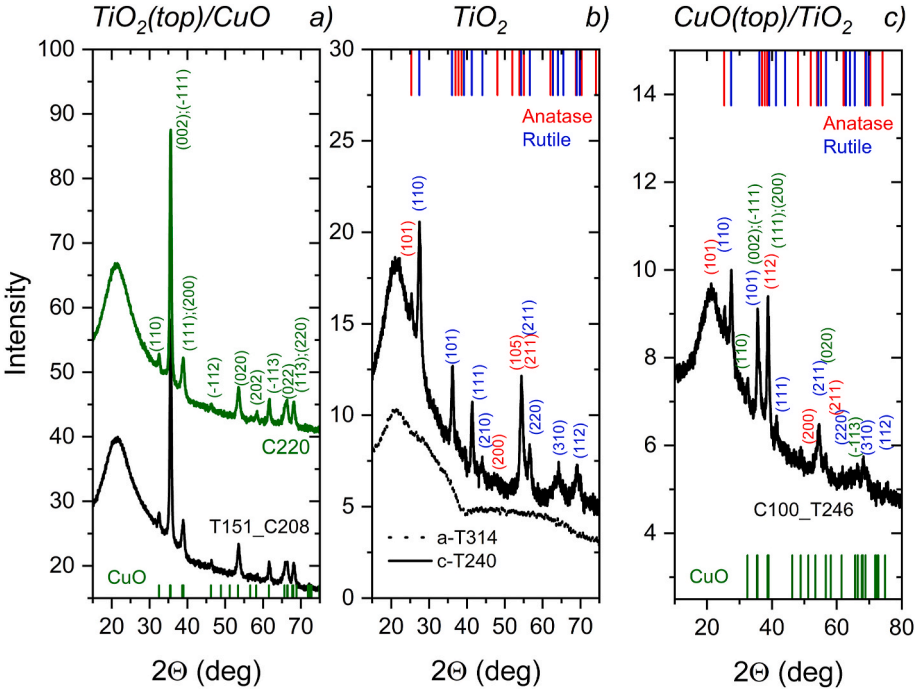

Fig. 2. XRD patterns for CuO and TiO_2(top)/CuO a), amorphous TiO_2 (a-T314) deposited at room temperature and crystallized TiO_2 (c-T240) in a form of anatase and rutile mixture deposited at 350 °C b) and for CuO(top)/TiO_2 c) together with reflexes from both monoclinic CuO and TiO_2 in a form of anatase and rutile.

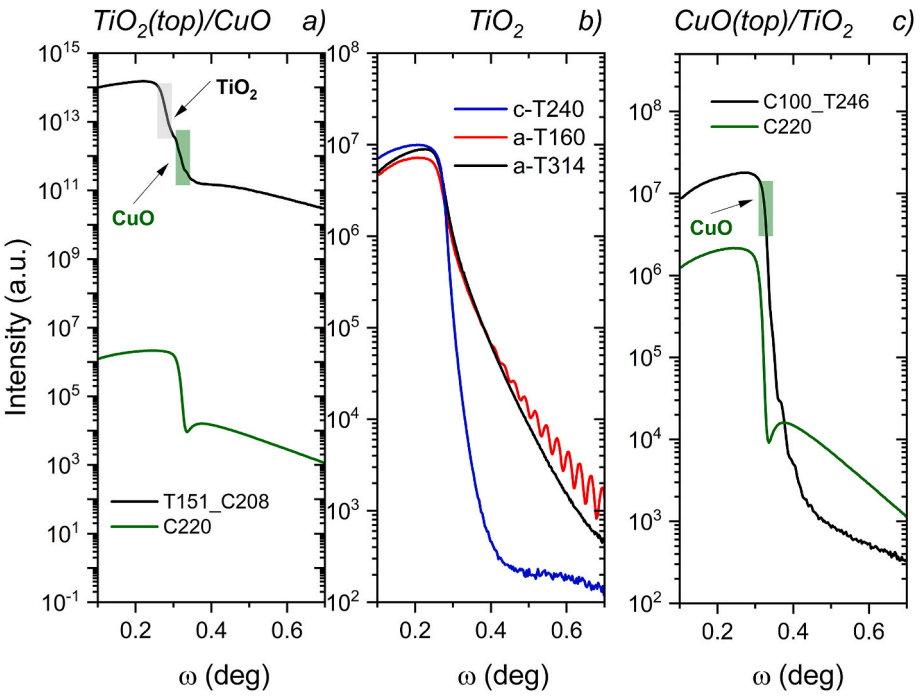

Fig. 3. X-ray reflectivity results for CuO (C220) and TiO_2(top)/CuO a), amorphous TiO_2 with different thicknesses (160 and 314 nm) deposited at room temperature and crystallized TiO_2 (c-T240) deposited at 350 °C b) and CuO together with CuO(top)/TiO_2 c).

Microscopy SEM (Helios G4 PFIB CXe DualBeam) while the elemental chemical analysis was performed with the use of EDS detector - Quanta XFlash 630 EDS, Bruker. High Resolution Transmission Electron Microscope (HR-TEM) JEOL F2000 cFEG TEM 200 kV served for imaging the surface and cross-sections of the lamellas prepared with the use of Focused Ion Beam. Optical properties were analysed through measurement of transmittance and reflectance spectra registered by a double beam Lambda 19 UV–VIS spectrophotometer (PerkinElmer). Functional properties were tested in the PhotoElectrochemical Cell (PEC) as photocurrent kinetics in a three-electrode cell (CuO; TiO_2; CuO(top)/-TiO_2; TiO_2(top)/CuO thin film as a working electrode, Pt covered with platinum black as an auxiliary electrode and Ag/AgCl/3 M KCl as a reference electrode). The measurement of photocurrent at 0 V was performed upon white light generated by Xe lamp (on/off pulses) of 150 W.

3. Results and discussion

The analysis of the results is based on comparison of two types of heterojunctions with each other and with single thin films of TiO_2 and CuO. Crystal structure of TiO_2(top)/CuO and CuO(top)/TiO_2 thin film bilayers was analysed based on X-ray diffraction patterns presented in Fig. 2. For the TiO_2(top)/CuO heterostructure composed of copper oxide covered with titanium dioxide it is a clearly visible that only one crystal phase could be identified, i.e., monoclinic CuO (ICDD 01-080-1268). The result of measurement reflects the shape of the pattern corresponding to a single CuO thin film. The reflexes from the second constituent of the bilayer – TiO_2 – could not be observed in the pattern, because of the room temperature during deposition. In order to obtain one of the crystalline forms of TiO_2: anatase, rutile or brookite, it is necessary to carry out synthesis at an elevated temperature above 350 °C [21–24] while CuO crystallizes even at room temperature. Fig. 2b presents the results for TiO_2 sputtered by rf reactive magnetron sputtering at room temperature - amorphous TiO_2 (a-T314) and crystallized form of TiO_2 deposited at 350 °C (c-T240). The first pattern confirms the amorphous nature of the thin film deposited without heating the substrates. Sample obtained at 350 °C crystallizes in the form of mixture of anatase (ICDD 01-078-2486) and rutile (ICDD 01-086-0147). The result of X-ray diffraction analysis for CuO(top)/TiO_2 (Fig. 2c) is the combination of pattern corresponding to monoclinic phase of CuO and TiO_2 rutile/anatase.

X-ray reflectivity, XRR is another method dedicated to thin film bilayers analysis through determination of density, roughness and thickness of the individual layers. Reflectivity is measured as a function of the angle of incidence ω between the thin film surface and X-ray beam direction. Roughness can be analysed based on how fast the curve drops near the critical angle for a single layer. In the bilayer systems the roughness of the interface between both components could be studied. Drop of intensity at the critical angle gives the information about density [25,26]. Fig. 3 presents the XRR curves for TiO_2(top)/CuO bilayer (T151_C208) and CuO thin film (C220), TiO_2 in crystallized (c-T240) and amorphous forms of thin films with different thicknesses (a-T160 and a-T314) and CuO(top)/TiO_2 bilayer (C100_T246) and CuO thin film (C220). Results presented in Fig. 3a for CuO thin film are characterized by a single drop in the intensity at the critical angle, while for the T151_C208 sample, two drops could be observed due to the advantageous arrangement of thin films, when CuO is covered by TiO_2. In between, there is an interference pattern of X-rays at the interface of TiO_2 and CuO layer. The beneficial arrangement of the layers is that the material with the higher density is below, thanks to which both critical angles can be indicated on the reflectivity curve. Theoretical density of CuO is equal to 6.51 g/cm^3, 4.31 g/cm^3 for TiO_2 rutile and is 3.89 g/cm^3 for TiO_2 anatase. Reflectivity spectra corresponding to single TiO_2 thin films in crystallized and amorphous forms is presented are Fig. 3b. Crystallized form of TiO_2 (c-T240) is characterized by the highest roughness which is manifested by the most pronounced decease in the intensity. For the amorphous TiO_2 the drop of intensity changes a bit slower, which confirms that these layers are characterized by smooth surface. Kiessig fringes are clearly visible for a sample with smaller thickness (a-T160) in contrast to thin film with thickness of 314 nm (a-T314). For an inverse type of heterostructure, CuO(top)/TiO_2 (Fig. 3c), only one drop of the intensity at the critical angle for CuO and then interferences assigned to CuO could be observed. Therefore, the drop of intensity corresponding to TiO_2 characterized with smaller

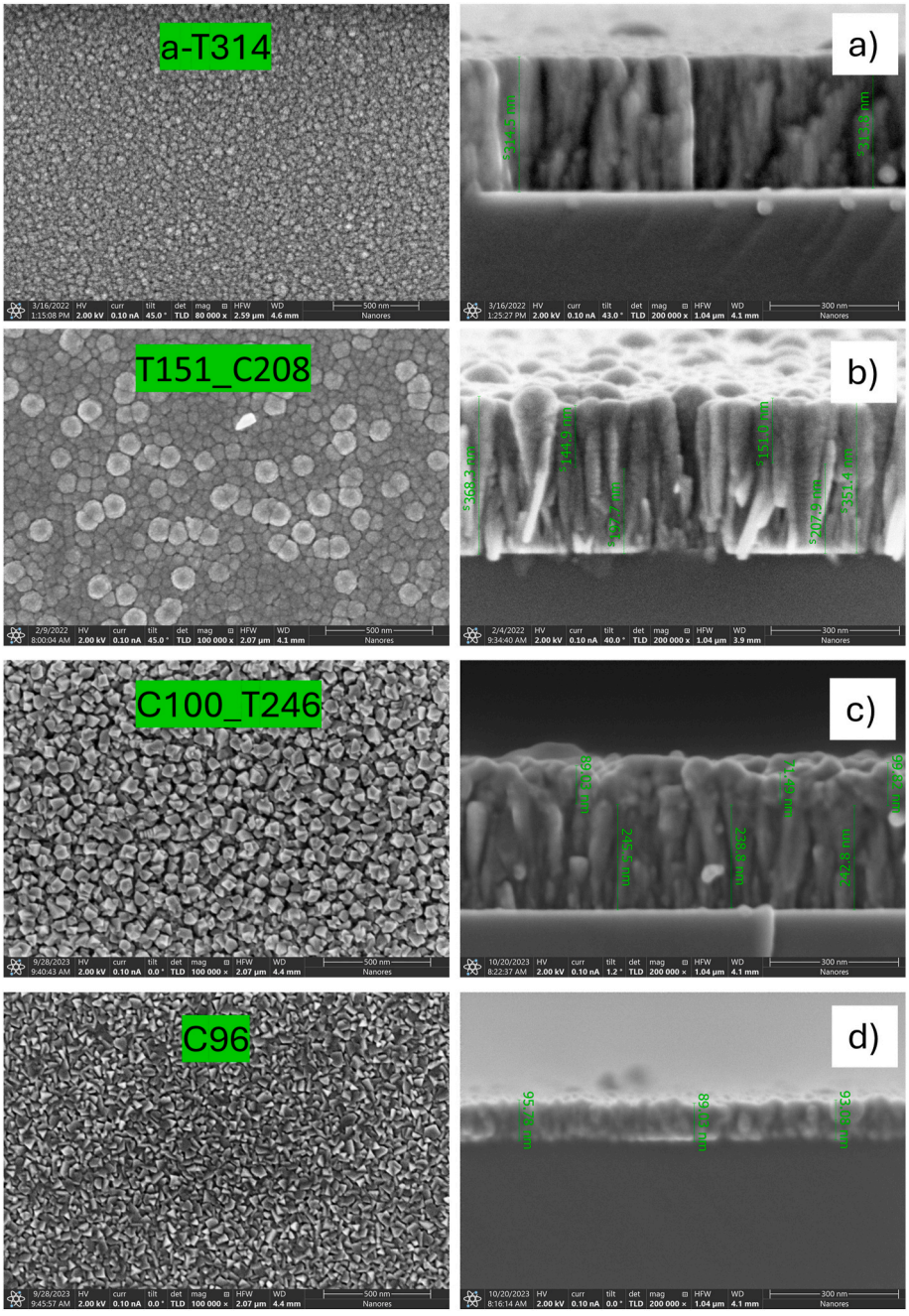

Fig. 4. SEM images of top view and cross section of thin films obtained by rf reactive magnetron sputtering: amorphous TiO_2 a), TiO_2(top)/CuO b), CuO(top)/TiO_2 c) and CuO d).

density could not be indicated. Moreover, the bilayer was obtained at the temperature equal to 350 °C and thus the surface of the bilayer is characterized by high roughness. This effect causes a sharp change in the reflectivity, what finally disrupts the visibility of interference.

Morphology and mode of growth of thin films could be analysed based on SEM images in the form of top views and cross sections presented in Fig. 4 for a single layer of amorphous TiO_2, TiO_2(top)/CuO, CuO(top)/TiO_2 and CuO. Amorphous TiO_2 presented in Fig. 4a is composed of uniformly distributed small elements without defined shape. The single layer is compact, smooth and uniform in thickness. The deposition performed at room temperature does not ensure the conditions for crystallization, which agrees with the above mentioned XRD and XRR results. The bilayer TiO_2(top)/CuO (Fig. 4b) was created as a result of covering copper oxide thin film of about 200 nm with the titanium oxide layer of about 150 nm. TiO_2 was deposited at room temperature onto a copper oxide thin film leading to formation of a spherically shaped grains with voids in between. Due to the amorphous nature of the top layer, the interface between two constituents of the heterostructure could be easily pointed out. The inverse of that bilayer in the form of CuO(top)/TiO_2 (Fig. 4c) sputtered on the heated substrates crystallized as mentioned above in the form of monoclinic CuO on top of TiO_2 layer in anatase and rutile form. Top surface of the bilayer is similar to that of a CuO single layer (Fig. 4d), however the copper oxide grown on TiO_2 bottom layer is characterized by more rounded shape in comparison to pyramids of a single CuO. The interface between both components of the heterostructure is less clear than in a case of that shown in Fig. 4b. There are several works which demonstrate that copper oxide morphology strongly depends on the synthesis conditions

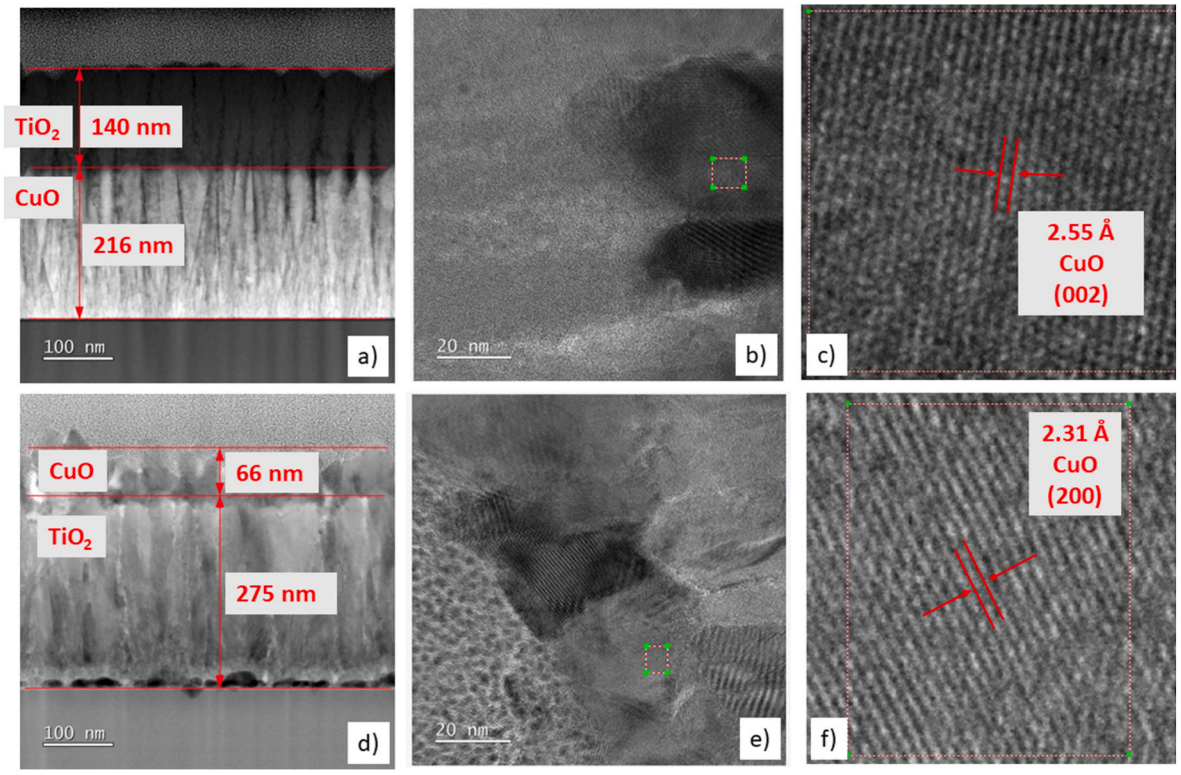

Fig. 5. HR-TEM images with analysis of interplanar distances for TiO_2(top)/CuO (a–c) and CuO(top)/TiO_2 bilayers (d–f).

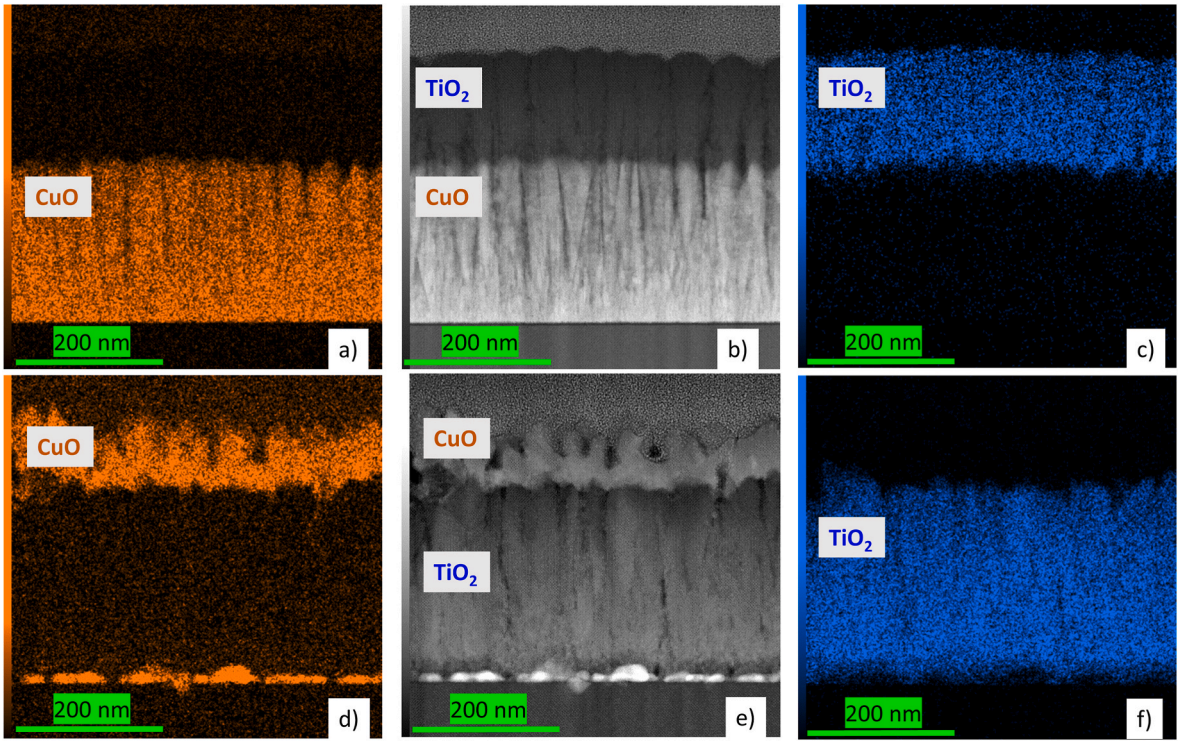

Fig. 6. Cross-section HR-TEM images of thin film bilayers along with EDS elemental mapping on the cross section of TiO_2(top)/CuO bilayer (a–c) and CuO(top)/TiO_2 (d–f).

[27–29]. Moreover, functional properties of the material, depending on the physical properties of thin films such as electronic structure, carrier concentrations and mobilities, can also be tuned through changing of the deposition conditions such as oxygen concentration in the reactive gas mixture [30–32].

Fig. 5 present HR-TEM images of TiO_2(top)/CuO and CuO(top)/TiO_2 together with thickness markers and interplanar distances for CuO calculated from HRTEM images. TiO_2(top)/CuO bilayer is composed of

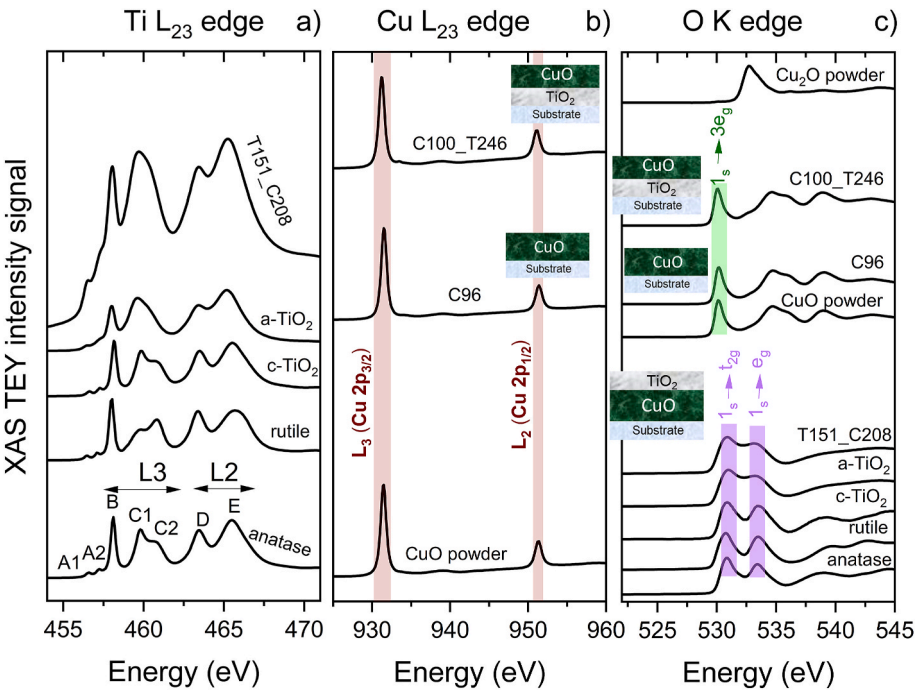

Fig. 7. X-ray absorption XAS spectra measured in Total Electron Yield (TEY) mode at Ti L_{23} edge for thin films (TiO_2(top)/CuO, amorphous TiO_2 and crystallized TiO_2) and powders (rutile, anatase) a), at Cu L_{23} edge for thin films (CuO(top)/TiO_2, CuO) and reference powder (CuO) b) and at O K edge for thin films (TiO_2(top)/CuO, amorphous TiO_2 and crystallized TiO_2, CuO, CuO(top)/TiO_2) and powders (rutile, anatase, CuO and Cu_2O) c). Bands for TiO_2 [40–44] and CuO [45] were marked based on literature.

the bottom CuO of 216 nm thickness, and the top TiO_2 with thickness of about 140 nm. CuO(top)/TiO_2 with inverted configuration is composed of 275 nm of TiO_2 and 66 nm of CuO at the top. Both SEM images (Fig. 4c) and cross-section TEM image (Fig. 5d) clearly indicate that the surface of the CuO(top)/TiO_2 consists of grains with visible empty spaces between them. Surface morphology formed in that way influences the roughness and overall density of heterojunction which could be calculated based on the fitting of a reflectivity curve. XRR pattern for TiO_2(top)/CuO thin film was fitted with the 5 layers and the density of the last one was equal to 5.6 g/cm^3, while for CuO(top)/TiO_2 bilayer the fitting included three layers and the roughness of the top layer was of about 6.3 nm. In both heterostructures interplanar distances corresponding to CuO monoclinic phase (ICDD 01-080-1268) were found, which is in agreement with XRD results (Fig. 2a–c).

Fig. 6 constitutes a comparison of HR-TEM cross section images of TiO_2(top)/CuO and CuO(top)/TiO_2 together with EDS elemental mapping for Cu and Ti. The elemental composition of thin films was presented in a form of colors for copper and titanium, thus, it was possible to indicate areas of copper oxide and titanium oxide on the cross-sections. The result allows us to conclude that both elements are evenly distributed regardless of the bilayer configuration. For TiO_2(top)/CuO (Fig. 6a–c) the most compact and dense part of CuO film is located near the silicon substrate; above this layer, gaps of varying lengths separating the long columns of copper oxide begin to be visible. The top layer of the system consists of amorphous titanium dioxide, in which the cracks are still present but are slightly less visible, suggesting that the pores originating from the bottom layer are rather developed near the interface. The second type of heterostructure CuO(top)/TiO_2 (Fig. 6d–f) is composed of a thick layer of TiO_2 covered with a thin layer of CuO with irregular shape and thickness. There are some voids in the TiO_2 layer, whereas the upper layer, although relatively thin is well developed. For this type of heterojunction, CuO(top)/TiO_2, which was obtained at 350 °C one can indicate some islands of copper located near the silicon substrate, which may be due to copper diffusion at high temperature. The phenomenon of copper diffusion in thin films under the elevated temperatures is widely described in literature [33–38]. For both types of heterostructure the interface between constituents is clearly visible (Fig. 6b–e).

Among different element specific techniques, X-ray absorption spectroscopy, XAS may be used to study the local atomic structure, coordination number, valence state, and hybridization of the atoms under investigation. X-ray absorption spectra reflect the density of empty/partially filled electronic states while following the excitation of an inner shell electron to the states that are allowed by the dipole selection rules. X-ray absorption spectroscopy XAS in TEY mode, similarly to X-ray photoelectron spectroscopy, XPS, probes the upper layer of the samples, up to several nanometers, only. Both techniques allow to study the electronic structure of the film surface. However, in the case of copper oxides, XAS when compared with XPS, decidedly gives unequivocal results as far as the valence state of Cu ions is concerned. Therefore, XAS analysis instead of XPS was employed for the purposes of this work. The XAS spectra of TiO_2(top)/CuO and CuO(top)/TiO_2 bilayers are presented in Fig. 7 within the energy ranges corresponding to L_{23} lines of Ti (Fig. 7a), and those of Cu (Fig. 7b) as well as K edge of oxygen (Fig. 7c). Titanium L edge, composed of two structures L_3 and L_2 visible in Fig. 7a, results from $2p^63d^n \rightarrow 2p^53d^{n+1}$ transitions accompanied by spin-orbit splitting of 2p state into $2p_{3/2}$ and $2p_{1/2}$. Similar splitting is observed in the case of Cu L spectrum (Fig. 7b) but the separation between L_2 and L_3 peak positions is much bigger, i.e., 20–21 eV for CuO and 5–6 eV for TiO_2. Moreover, the crystal field splitting of Ti3d orbitals into lower-energy (t_{2g}) and higher-energy (e_g) suborbitals is responsible for further development of double-peak structures of both L_3.and L_3 lines, denoted as B, C for L_3 and D, E for L_2 in Fig. 7a. This effect does not take place for CuO as seen in Fig. 7b. X-ray absorption spectra of well-crystallized rutile and anatase TiO_2 powders display additional splitting of C peak into C_1 and C_2 the intensity ratio of which is different for anatase and rutile. This effect has been previously attributed to the differences in energy of $d_{x^2} - d_{y^2}$ and d_{z^2} orbitals [39] and serves as a fingerprint of polymorphic forms of TiO_2. Therefore, interpretation of the more complex XAS spectrum for TiO_2(top)/CuO

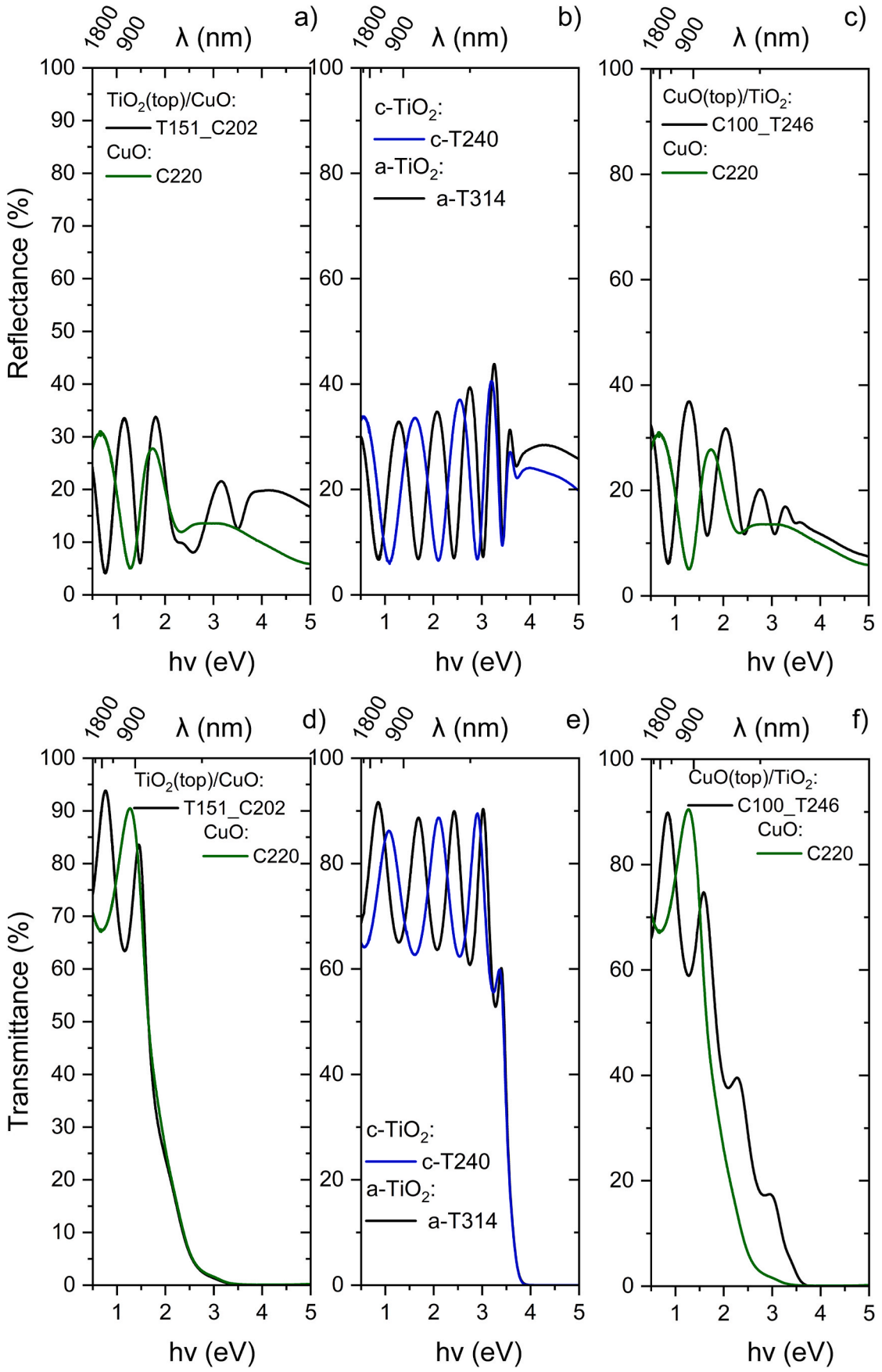

Fig. 8. Reflectance a–c) and transmittance d–f) spectra of CuO and TiO_2(top)/CuO, amorphous TiO_2 deposited at room temperature and crystallized TiO_2 deposited at 350 °C and of CuO together with CuO(top)/TiO_2.

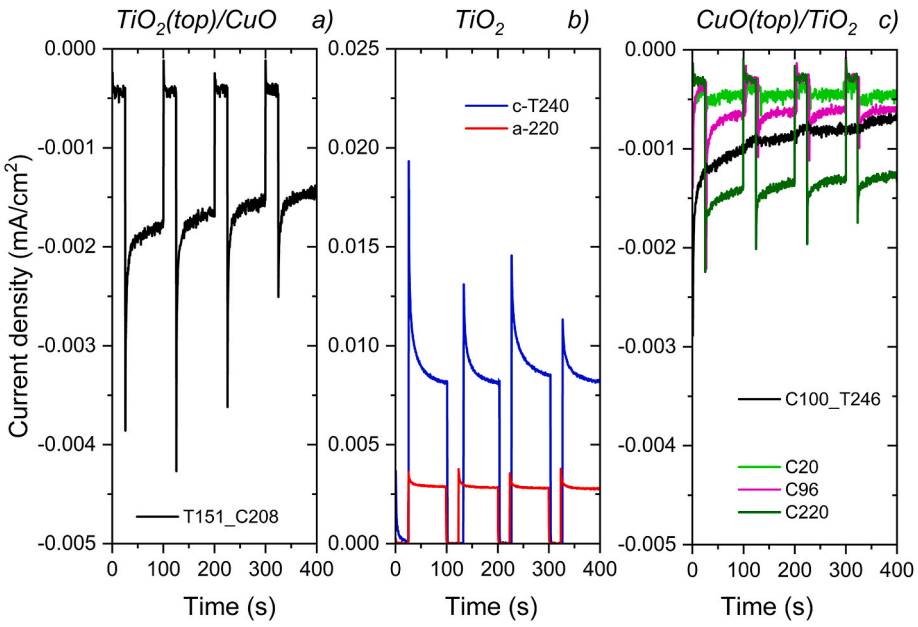

Fig. 9. Photocurrent I_{ph} kinetics of thin film electrodes: TiO_2(top)/CuO a), amorphous TiO_2 (a-220) and crystallized TiO_2 (c-T240) b) and CuO(top)/TiO_2 c).

sample (Fig. 7a) can be done by comparing it with the spectra of TiO_2 powders, c-TiO_2 crystalline and a-TiO_2 amorphous single layers. Ti L_{23} XAS spectrum of TiO_2(top)/CuO bilayer resembles that of a-TiO_2 especially within the range of energies where the splitting of C peak into C_1 and C_2 is typically seen in the case of anatase, rutile and c-TiO_2. The lack of splitting remains in accordance with the XRD results presented in Fig. 2a that indicates the amorphous character of TiO_2 top layer grown on crystalline CuO. Cu L_{23} edge of the CuO(top)/TiO_2 bilayer is less complicated and contains two peaks, only (Fig. 7b). Comparison with the CuO powder and single layer spectra confirms that Cu^{2+} species are present at the bilayer surface. Major features of the O K-edge X-ray absorption spectra of various transition metal oxides including TiO_2 and CuO can be accounted for by the molecular orbital theory. According to this theory, the main peaks in Fig. 7c illustrate the transitions from O1s to hybridized O2p levels. For crystalline TiO_2, because of the crystal field splitting into t_{2g} and e_g states two well-resolved peaks $1s \rightarrow t_{2g}$ and $1s \rightarrow e_g$ can be seen. For amorphous TiO_2 and TiO_2(top)/CuO sample with amorphous TiO_2 top layer, the separation of these peaks becomes less-pronounced. In the case of CuO samples or CuO(top)/TiO_2 bilayers, the leading O K edge contains only one narrow peak at slightly lower photon energy corresponding to $1s \rightarrow 3e_g$ transitions. This result confirms Cu^{+} presence at the film surface.

Optical properties of TiO_2(top)/CuO and CuO(top)/TiO_2 bilayers as well as those of single TiO_2 and CuO thin films have been determined from the spectrophotometric measurements of reflectance and transmittance coefficients over uv, visible and near-infrared ranges of photon energies hν as shown in Fig. 8. Among many technological parameters that influence the transmittance and reflectance spectra of thin films, their thickness produces the most spectacular effect. The multiple interference of light reflected from air-film and film-substrate interfaces is responsible for the oscillating character of all the curves presented in Fig. 8. For single layers of CuO and TiO_2 it is relatively easy to interpret these spectra. The most important difference, clearly seen when comparing the transmittance spectra (Fig. 8d and e), is the position of the fundamental absorption edge that is shifted to longer wavelengths in the case of CuO which is a narrow band semiconductor [46]. Therefore, one can expect much more efficient absorption of light within the visible range when combining TiO_2 – a wide band semiconductor with CuO in the heterostructure that should affect the performance of photoelectrodes in green hydrogen generation.

Surface roughness is yet another significant factor related to the film morphology the influence of which can be followed from the reflectance spectra at photon energies higher than the band gap E_g. Decreased surface roughness when covering CuO with TiO_2 (Fig. 8a) results in less pronounced light scattering and higher reflectance coefficient at $h\nu > 2$ eV. Moreover, within the optical window between 2 eV and 4 eV ($E_g(CuO) < h\nu < E_g(TiO_2)$) the interference of light takes place for both types of bilayers, i.e., TiO_2(top)/CuO and CuO(top)/TiO_2 which manifests itself in oscillations in the reflectance (Fig. 8 a and c) as well as in the transmittance coefficients (Fig. 8d and f). The conclusions concerning the surface roughness drawn from optical spectra of amorphous and crystalline TiO_2 single layers (Fig. 8 b and e) remain in accordance with the XRR results presented in Fig. 3b.

Fig. 9 illustrates the time dependence of photocurrent intensity I_{ph} when white light is abruptly switched on and off. The photocurrent kinetics presented in Fig. 9 have been recorded for photoelectrodes based on titanium dioxide and copper oxide, as well as their bilayer systems. The sudden change in photocurrent and subsequent steady-state value can be attributed to the separation of the electron-hole pair generated by the illumination. An increase in the anodic photocurrent (positive I_{ph} values) is observed exclusively in the case of TiO_2 electrodes (Fig. 9b). The use of titanium dioxide layers with a crystalline structure (c-T240) has been observed to result in a more than twofold increase in the photocurrent as compared to the amorphous material (a-220). Negative photocurrent values, both in the dark and upon illumination, are observed for copper oxide, indicating that the electrodes tested exhibit cathodic behaviour. Photoelectrodes in the form of bilayers, regardless of their configuration CuO/TiO_2 or TiO_2/CuO, also exhibit cathodic behaviour, whereby the current takes on negative values.

The influence of the thicknesses of the TiO_2 and CuO layers, within the range of 20–250 nm, on the photocurrent values is demonstrated in Fig. 10a and b, respectively. In the range of electrode materials thicknesses that were studied, an increase in photocurrent values was observed with the increasing thickness. The impact of layer thickness on photoelectrochemical characteristics, including photocurrent values, is well documented in the literature [47]. This influence is not limited to the type of semiconductor but also extends to its structural and microstructural properties. Hao et al. explained the photocatalytic mechanism for CuO covered with TiO_2 by finding the relationship between thickness of both components, porosity and specific surface area [15]. Furthermore, regardless of the thickness of the oxides, the anodic character of the TiO_2 and the cathodic character of the CuO electrodes was

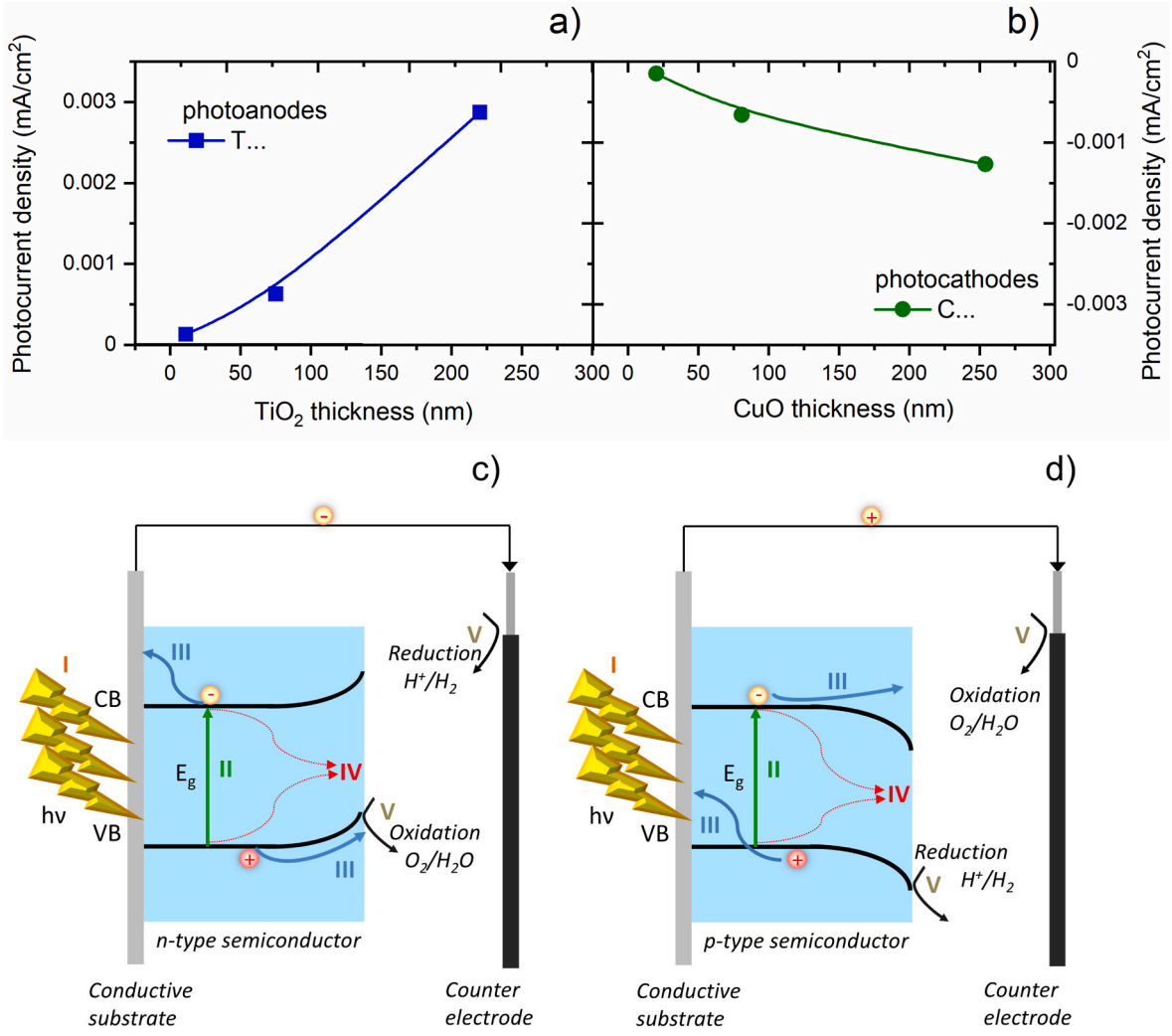

Fig. 10. Photocurrent densities calculated based on photocurrent kinetics versus CuO and TiO_2 thin films thicknesses for TiO_2 photoanodes a) and CuO photocathodes b). Schematic representation of the processes occurring upon illumination of the n-type c) and p-type d) semiconductor electrode included in the PEC PhotoElectrochemical Cell, where: I – light absorption, II – carriers separation, III – charge transport, IV – carriers recombination, V – redox reactions, CB – conduction band, VB – valence band, E_g – band gap. Graphics prepared based on the reference [48].

maintained. The photoelectrolysis of water is conducted in a Photo-Electrochemical Cell (PEC), the key component of which is a semiconductor photoelectrode. Fig. 10c and d illustrate schematically the processes that take place in the PEC. Upon illumination of a semiconductor with light of photon energy hν > Eg, electrons in the conduction band (CB) and electron holes in the valence band (VB) are created (Fig. 10c d).

This process can be described with the following reaction:

$$h\nu \Rightarrow e' + h^{\cdot} \quad (1)$$

where hν is photon energy, e' the electron and $h^{\cdot}$ the electron hole. The charge carriers can be used to drive a chemical reaction of photoelectrolysis. Electrons (e') participate in the reduction reaction:

$$2H^{+} + 2e' \Rightarrow H_{2(gas)} \quad (2)$$

and holes ($h^{\bullet}$) oxidize water:

$$2h^{\cdot} + H_2O \Rightarrow \frac{1}{2}O_2 + 2H^{+}. \quad (3)$$

The reduction of hydrogen ions to hydrogen gas or oxidation of water to oxygen gas are observed at the anode or cathode, respectively, with the type of conductivity exhibited by the photoelectrode material being a determining factor.

In the case of n-type semiconductor (Fig. 10c), which acts as a photoanode, the electrons are transported over an external circuit to the cathode, where hydrogen is generated via the reduction of water. Photoinduced holes take part in the anode reaction that occurs at the semiconductor/electrolyte interface. In contrast (Fig. 10d), the application of a p-type semiconductor results in the generation of hydrogen at the surface of the photocathode and oxygen at the anode (counter electrode).

Systems in the form of bilayers with different configurations, namely CuO(top)/TiO_2 or TiO_2(top)/CuO, were employed as photoelectrodes in a PEC cell. The obtained results of photocurrent density values for PECs without external polarisation are presented in Fig. 11. The photocurrent values for TiO_2/CuO double layers with 208 nm copper oxide and variable TiO_2 top layer thickness are higher than those for the reverse system CuO/TiO_2. In fact, the photocurrent for the bilayers where a 20 nm CuO top layer is used is the lowest of all. However, increasing the CuO layer thickness to 100 nm for the CuO/TiO_2 system results in an improvement.

In order to explain the photoelectrode performance the mechanism was proposed for two types of bilayer system: TiO_2(top)/CuO and CuO (top)/TiO_2. Fig. 12 shows the band energy structure of the CuO/TiO_2 and TiO_2/CuO bilayer under illumination. The edges of the conduction

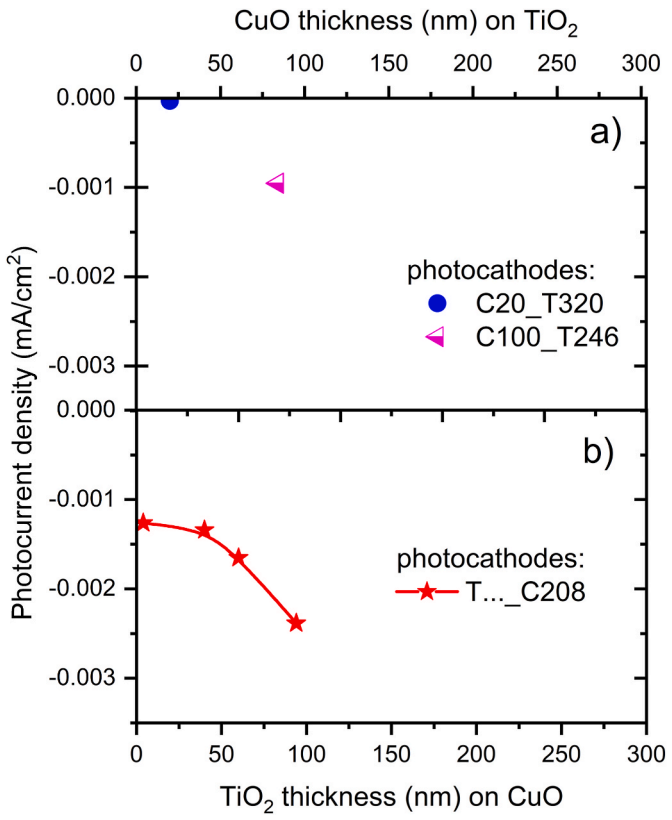

Fig. 11. Photocurrent densities calculated based on photocurrent kinetics versus CuO and TiO_2 thin films thicknesses for CuO(top)/TiO_2 a) and TiO_2(-top)/CuO bilayers b).

and valence bands of p-type CuO are at a higher level compared to the corresponding bands of n-type TiO_2. This is due to the different types of conductivity and differences in forbidden energy values. In the TiO_2/CuO system, light-induced electrons in the conduction bands of both oxides can be injected into water, causing its reduction. This differs from the CuO/TiO_2 system, where only photoelectrons from CuO are involved in this reaction. A similar phenomenon is observed for h^+ photocarriers. In this case, however, only the holes from the valence band of TiO_2 are directed towards the ITO substrate and then through the outer circuit to the anode, where they participate in the oxidation reaction. The enhanced photoactivity of the TiO_2/CuO bilayer for PEC can be attributed to the following processes. First, the photocarriers formed in both oxides are involved in oxidation-reduction reactions. In addition, the growth of the CuO layer on the ITO substrate is characterised by an optimal interface, which facilitates the transfer of photocarriers to the substrate. The interface for TiO_2(top)/CuO bilayer is created as a result of covering rough bottom layer of CuO with smooth top surface of TiO_2. Inverse configuration, CuO(top)/TiO_2, is a heterojunction originated from rough bottom layer coated with rough top surface. The interface between two semiconductors for TiO_2(top)/CuO heterostructure also allows for efficient electron flow from CuO to TiO_2.

Recently published works related to heterojunctions based on titanium dioxide and copper oxide with different architectures were collected in Table 2. The materials presented in the literature review are prepared mostly by multi-stage processes. Thin films heterostructures presented in this work were obtained by sequential sputtering carried out without breaking a vacuum which allows to grow bilayers with a well-defined interface between both components.

4. Conclusions

In summary, two types of thin film bilayers with configuration TiO_2(top)/CuO and CuO(top)/TiO_2 were obtained by means of reactive rf magnetron sputtering. The strategy that guarantees obtaining a bilayer with well-defined interface was to apply sequential deposition without breaking the vacuum. TiO_2(top)/CuO bilayer was created as a result of covering rough bottom layer of CuO with smooth top surface of TiO_2. Inverse configuration, CuO(top)/TiO_2, was a heterojunction originated as rough bottom layer coated with rough top surface. CuO in both types of bilayers is monoclinic, while TiO_2 crystallizes in the form of mixture of anatase and rutile at CuO(top)/TiO_2. TiO_2 remains amorphous after deposition at room temperature during inverse configuration preparation. Finding the correlation between structural, optical properties, surface morphology and photoelectrochemical performance of bilayers with diverse configurations allowed to identify the conditions which provide more efficient photoelectrochemical reactions in the case of TiO_2(top)/CuO over inverse configuration. Photocurrent kinetics revealed that both types of bilayer photoelectrodes exhibited cathodic character, and the current was a function of layer thickness. The

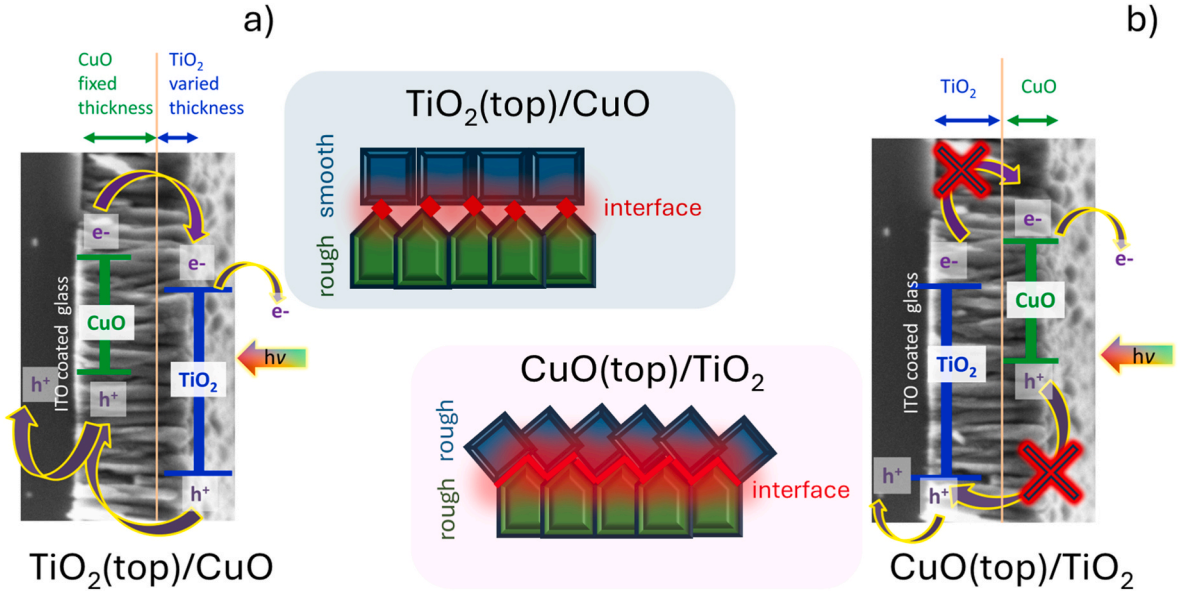

Fig. 12. Proposed mechanism for two types of bilayer system: TiO_2(top)/CuO a) and CuO(top)/TiO_2 b) together with the architecture of the interface.

Table 2
Heterojunctions based on titanium dioxide and copper oxide with different architectures for application in water splitting and photocatalysis.

System	Architecture	Form	Method of preparation (sensitization)	Application	Ref.
Cu_2O/TiO_2	p-n heterojunction, type II	powder: composite	ball milling	photocatalytic hydrogen generation	[49]
$CuO/TiO_2/Ti$	p-n heterojunction	thin film: TiO_2 nanotube arrays covered with CuO nanoparticles	Ti foil anodization, thermal decomposition $Cu(NO_3)_2$	photoelectrocatalytic hydrogen evolution and pollutant removal	[50]
Cu_2O/TiO_2/FTO CuO/TiO_2/FTO TiO_2/CuO/FTO	S-scheme heterojunction	thin film: TiO_2 nanorods covered with CuO and Cu_2O	hydrothermal synthesis of TiO_2, SILAR deposition of Cu_2O (calcination leading to CuO); CuO covered with TiO_2 by spin coating method	solar water splitting and photocatalytic CO_2 reduction	[51]
$CuO_x/TiO_2/Ti$	heterojunction	thin film: TiO_2 nanotubes, modified with CuO_x	Ti foil anodization, Cu sputtered and thermally-treated under hydrogen atmosphere or conventionally annealed in a tube furnace	photocatalytic CO_2 reduction reaction	[52]
front contact/ CuO/TiO_2	p-n heterojunction, type II	thin film	numerical analysis	photocatalytic hydrogen generation	[53]
CuO/TiO_2	heterojunction	powder: composite	TiO_2 powder thermally treated with Cu, Mechanically mixed and then calcined	photocatalytic hydrogen generation	[54]
CuO/TiO_2/FTO	heterojunction, type II	thin film: TiO_2 nanorods covered with CuO	two steps hydrothermal process and calcination	photoelectrochemical hydrogen generation	[55]
CuO_x/TiO_2	heterojunction, type II	powder	impregnation and calcination, electrophoretic deposition on FTO and annealing	photocatalytic H_2 generation, photocatalytic CO_2 reduction	[56]
CuO_x-TiO_2-N-doped carbon	heterojunction	powder	N-doped carbon (NC) – chemical synthesis and calcination; TiO_2-hydrothermal; CuO_x-TiO_2-wet impregnation; CuO_x-TiO_2-NC – grinding and calcination	oxygen reduction reaction	[57]
CuO–TiO_2	heterojunction	thin film	CuO: chemical and electrochemical methods; CuO–TiO_2: Spin coating	photoelectrochemical hydrogen production	[58]

mechanism of the photoelectrode performance was proposed for both types of heterostructure: TiO_2(top)/CuO is a type II heterostructure, while for inverse configuration charge transfer between semiconductors does not occur, thus causes the limitation in the overall efficiency of redox reactions.

CRediT authorship contribution statement

Joanna Banaś-Gac: Writing – original draft, Visualization, Validation, Project administration, Methodology, Investigation, Funding acquisition, Formal analysis, Data curation, Conceptualization. **Marta Radecka:** Writing – original draft, Validation, Supervision, Methodology, Conceptualization. **Eduard Llobet:** Supervision, Investigation. **Ewa Partyka-Jankowska:** Investigation. **Katarzyna Zakrzewska:** Writing – original draft, Validation, Supervision, Project administration, Methodology, Funding acquisition, Conceptualization.

Declaration of competing interest

The authors declare that they have no known competing financial interests or personal relationships that could have appeared to influence the work reported in this paper.

Acknowledgements

Research supported by program “Excellence initiative – research university” (KZ acknowledges grant ID. 4149 Action 4 and JBG acknowledges grant ID. 7399 Action 6) for the AGH University of Krakow.

X-ray absorption experiment entitled “Temperature evolution of the electronic structure of Cu_2O/CuO_x and TiO_2/CuO_x bilayered thin films studied in situ by XAS” (no. 233016) was performed at PIRX beamline of National Synchrotron Radiation Centre SOLARIS, the access to which was provided by the project of Polish Ministry of Science and Higher Education under contract no. 1/SOL/2021/2.

Valuable contribution of Dr Adam Czapla related to the interpretation of optical measurements and Dr Edward Kusior for XRD and XRR measurements is highly appreciated.

References

[1] Martínez de León C, Molina P, Ríos C, Brey JJ. Green hydrogen production’s impact on sustainable development goals. Int J Hydrogen Energy 2025. https://doi.org/10.1016/j.ijhydene.2024.12.355.
[2] Kovač A, Paranos M, Marciuš D. Hydrogen in energy transition: a review. Int J Hydrogen Energy 2021;46:10016–35. https://doi.org/10.1016/j.ijhydene.2020.11.256.
[3] Ajanovic A, Sayer M, Haas R. The economics and the environmental benignity of different colors of hydrogen. Int J Hydrogen Energy 2022;47:24136–54. https://doi.org/10.1016/j.ijhydene.2022.02.094.
[4] Hammi Z, Labjar N, Dalimi M, El Hamdouni Y, Lotfi EM, El Hajjaji S. Green hydrogen: a holistic review covering life cycle assessment, environmental impacts, and color analysis. Int J Hydrogen Energy 2024;80:1030–45. https://doi.org/10.1016/j.ijhydene.2024.07.008.
[5] Pathak PK, Yadav AK, Padmanaban S. Transition toward emission-free energy systems by 2050: potential role of hydrogen. Int J Hydrogen Energy 2023;48:9921–7. https://doi.org/10.1016/j.ijhydene.2022.12.058.
[6] Shiva Kumar S, Lim H. An overview of water electrolysis technologies for green hydrogen production. Energy Rep 2022;8:13793–813. https://doi.org/10.1016/j.egyr.2022.10.127.
[7] Kusoglu A. (Re)Defining clean hydrogen: from colors to emissions. Electrochem Soc Interface 2022;31:47–51. https://doi.org/10.1149/2.F08224IF.
[8] Choudhary S, Upadhyay S, Kumar P, Singh N, Satsangi VR, Shrivastav R, et al. Nanostructured bilayered thin films in photoelectrochemical water splitting - a review. Int J Hydrogen Energy 2012;37:18713–30. https://doi.org/10.1016/j.ijhydene.2012.10.028.
[9] Fujishima A, Honda K. Electrochemical photolysis of water at a semiconductor electrode. Nature 1972;238:37–8.
[10] Radecka M, Kusior A, Trenczek-Zajac A, Zakrzewska K. Oxide nanomaterials for photoelectrochemical hydrogen energy sources. Adv Inorg Chem 2018;72:145–83.
[11] Wang P, Wu H, Tang Y, Amal R, Ng YH. Electrodeposited Cu_2O as photoelectrodes with controllable conductivity type for solar energy conversion. J Phys Chem C 2015;119:26275–82. https://doi.org/10.1021/acs.jpcc.5b07276.
[12] Alotaibi AM, Muayqil E, Al Abass N, Alhajji MA, Bubshait AA, Alhazmi NE, et al. Surface engineering of CuO-Cu_2O heterojunction thin films for improved photoelectrochemical water splitting. Renew Energy 2024;235. https://doi.org/10.1016/j.renene.2024.121326.
[13] Zhang Z, Wang P. Highly stable copper oxide composite as an effective photocathode for water splitting via a facile electrochemical synthesis strategy. J Mater Chem 2012;22:2456–64. https://doi.org/10.1039/c1jm14478b.
[14] Wang P, Wen X, Amal R, Ng YH. Introducing a protective interlayer of TiO_2 in Cu_2O-CuO heterojunction thin film as a highly stable visible light photocathode. RSC Adv 2015;5:5231–6. https://doi.org/10.1039/c4ra13464h.
[15] Hao B, Guo J, Zhang L, Ma H. Magnetron sputtered TiO_2/CuO heterojunction thin films for efficient photocatalysis of Rhodamine B. J Alloys Compd 2022;903:163851. https://doi.org/10.1016/j.jallcom.2022.163851.
[16] Long M, Beranek R, Cai Wei-min, Kisch H. Hybrid semiconductor electrodes for light-driven photoelectrochemical switches. Electrochim Acta 2008;53:4621–6. https://doi.org/10.1016/j.electacta.2008.01.077.

[17] Kot A, Radecka M, Dorosz D, Zakrzewska K. Optically active TiO_2:Er thin films deposited by magnetron sputtering. Materials 2021;14. https://doi.org/10.3390/ma14154085.
[18] Kot A, Dorosz D, Radecka M, Zakrzewska K. Improved photon management in a photoelectrochemical cell with Nd-modified TiO_2 thin film photoanode. Int J Hydrogen Energy 2021;46:12082–94. https://doi.org/10.1016/j.ijhydene.2020.05.094.
[19] Banas-Gac J, Radecka M, Czapla A, Kusior E, Zakrzewska K. Surface and interface properties of TiO_2/CuO thin film bilayers deposited by rf reactive magnetron sputtering. Appl Surf Sci 2023;616. https://doi.org/10.1016/j.apsusc.2023.156394.
[20] Szlachetko J, Szade J, Beyer E, Błachucki W, Ciochoń P, Dumas P, et al. SOLARIS National Synchrotron Radiation Centre in Krakow, Poland. Eur Phys J Plus 2023;138:1–10. https://doi.org/10.1140/epjp/s13360-022-03592-9.
[21] Hanaor DAH, Sorrell CC. Review of the anatase to rutile phase transformation. J Mater Sci 2011;46:855–74. https://doi.org/10.1007/s10853-010-5113-0.
[22] Tanemura S, Miao L, Wunderlich W, Tanemura M, Mori Y, Toh S, et al. Fabrication and characterization of anatase/rutile-TiO_2 thin films by magnetron sputtering: a review. Sci Technol Adv Mater 2005;6:11–7. https://doi.org/10.1016/j.stam.2004.06.002.
[23] Vahl A, Dittmann J, Jetter J, Veziroglu S, Shree S, Ababii N, et al. The impact of O_2/Ar ratio on morphology and functional properties in reactive sputtering of metal oxide thin films. Nanotechnology 2019;30:235603. https://doi.org/10.1088/1361-6528/ab0837.
[24] Zakrzewska K, Brudnik A, Radecka M, Posadowski W. Reactively sputtered TiO_{2-x} thin films with plasma-emission-controlled departure from stoichiometry. Thin Solid Films 1999;343–344:152–5. https://doi.org/10.1016/S0040-6090(98)01651-4.
[25] Singh R, Gupta M, Phase DM, Mukherjee SK. Phase growth analysis of sputtered TiO_2 thin films at low oxygen partial pressures using XANES and XRR. Mater Res Express 2019;6:116449. https://doi.org/10.1080/14484846.2018.1432089.
[26] Holy V, Pietsch U, Baumbach T. High-resolution X-ray scattering from thin films and multilayers. Berlin: Springer; 1999. https://doi.org/10.1007/bfb0109385.
[27] Zheng W, Chen Y, Peng X, Zhong K, Lin Y, Huang Z. The phase evolution and physical properties of binary copper oxide thin films prepared by reactive magnetron sputtering. Materials 2018;11:1253. https://doi.org/10.3390/ma11071253.
[28] Hu J, Zou C, Su Y, Li M, Han Y, Siu-Wai Kong E, et al. Ultrasensitive NO_2 gas sensor based on hierarchical Cu_2O/CuO mesocrystals nanoflower. J Mater Chem A Mater 2018;6:17120–31.
[29] Rydosz A. The use of copper oxide thin films in gas-sensing applications. Coatings 2018;8. https://doi.org/10.3390/coatings8120425.
[30] Wang Y, Ghanbaja J, Soldera F, Migot S, Boulet P, Horwat D, et al. Tuning the structure and preferred orientation in reactively sputtered copper oxide thin films. Appl Surf Sci 2015;335:85–91. https://doi.org/10.1016/j.apsusc.2015.02.028.
[31] Alajlani Y, Placido F, Barlow A, Chu HO, Song S, Ur Rahman S, et al. Characterisation of Cu_2O, Cu_4O_3, and CuO mixed phase thin films produced by microwave-activated reactive sputtering. Vacuum 2017;144:217–28. https://doi.org/10.1016/j.vacuum.2017.08.005.
[32] Pierson JF, Thobor-Keck A, Billard A. Cuprite, paramelaconite and tenorite films deposited by reactive magnetron sputtering. Appl Surf Sci 2003;210:359–67. https://doi.org/10.1016/S0169-4332(03)00108-9.
[33] Butrymowicz DB, Manning JR, Read ME. Diffusion in copper and copper alloys. Part I. Volume and surface self-diffusion in copper. J Phys Chem Ref Data 1973;2:643–56. https://doi.org/10.1063/1.3253129.
[34] Chamberlain MB. Diffusion of copper in thin TiN films. Thin Solid Films 1982;91:155–62. https://doi.org/10.1016/0040-6090(82)90429-1.
[35] Raghavan G, Chiang C, Anders PB, Tzeng SM, Villasol R, Bai G, et al. Diffusion of copper through dielectric films under bias temperature stress. Thin Solid Films 1995;262:168–76. https://doi.org/10.1016/0040-6090(95)05839-7.
[36] Bacaksiz E, Dzhafarov TD, Novruzov VD, Öztürk K, Tomakin M, Küçükömeroğlu T, et al. Copper diffusion in ZnS thin films. Physica Status Solidi A 2004;201:2948–52. https://doi.org/10.1002/pssa.200306853.
[37] Chan R, Arunagiri TN, Zhang Y, Chyan O, Wallace RM, Kim MJ, et al. Diffusion studies of copper on ruthenium thin film a plateable copper diffusion barrier. Electrochem Solid State Lett 2004;7:154–7. https://doi.org/10.1149/1.1757113.
[38] Kuo YL, Lee HH, Lee C, Lin JC, Shue SL, Liang MS, et al. Diffusion of copper in titanium zirconium nitride thin films. Electrochem Solid State Lett 2004;7:1–4. https://doi.org/10.1149/1.1644355.
[39] De Groot FMF, Figueiredo MO, Basto MJ, Abbate M, Petersen H, Fuggle JC. 2p X-ray Absorption of Titanium in Minerals 1992;19. https://doi.org/10.1007/BF00202101.
[40] de Groot FMF, Fuggle JC, Thole BT, Sawatzky GA. 2p x-ray absorption of 3d transition-metal compounds: an atomic multiplet description including the crystal field. Phys Rev B 1990;42:410–3. https://doi.org/10.1103/PhysRevB.42.5459.
[41] de Grott FMF, Fuggle JC, Thole BT, Sawatzky GA. L2,3 x-ray absorption edges of d0 compounds: K^+, Ca^{2+}, Sc^{3+}, and Ti^{4+} in Oh (octahedral) symmetry. Phys Rev B 1990;41. https://doi.org/10.1103/PhysRevB.41.928.
[42] Hwu Y, Yao YD, Cheng NF, Tung CY, Lin HM. X-ray absorption of nanocrystal TiO_2. Nanostruct Mater 1997;9:355–8. https://doi.org/10.1016/S0965-9773(97)00082-2.
[43] Finkelstein LD, Zabolotzky EI, Korotin MA, Shamin SN, Butorin SM, Kurmaev EZ, et al. Vacant states of TiO_2 with rutile structure and their reflection in different-type x-ray absorption spectra. X Ray Spectrom 2002;31:414–8. https://doi.org/10.1002/xrs.596.
[44] Ruus R, Kikas A, Saar A, Ausmees A, Nommiste E, Aarik J, et al. Ti 2p and O 1s X-ray absorption of TiO_2 polymorphs. Solid State Commun 1997;104:199–203. https://doi.org/10.1016/S0038-1098(97)00300-1.
[45] Leapman RD, Grunes LA. Anomalous L_3/L_2 white-line ratios in the 3d transition metals. Phys Rev Lett 1980;45:397–401. https://doi.org/10.1103/PhysRevLett.45.397.
[46] Zoolfakar AS, Rani RA, Morfa AJ, O'Mullane AP, Kalantar-zadeh K. Nanostructured copper oxide semiconductors: a perspective on materials, synthesis methods and applications. J Mater Chem C Mater 2014;2:5247–70. https://doi.org/10.1039/C4TC00345D.
[47] Ansón-Casaos A, Ciria JC, Martínez-Barón C, Villacampa B, Benito AM, Maser WK. Modelling TiO_2 photoanodes for PEC water splitting: decoupling the influence of intrinsic material properties and film thickness. Int J Hydrogen Energy 2024;52:1146–58. https://doi.org/10.1016/j.ijhydene.2023.06.284.
[48] Jiangtian Li, Nianqiang Wu. Semiconductor-based photocatalysts and photoelectrochemical cells for solar fuel generation: a review. Catal Sci Technol 2015;5:1360–84.
[49] Umair M, Ruiz-Aguirre A, Berruti I, Rodríguez SM, Palmisano L, Loddo V, et al. Biomass derivatives photoreforming in pilot plant scale to obtain H_2 under green conditions by using ball milling Cu_2O-TiO_2 P25 photocatalysts. Chem Eng J 2025;504:158585. https://doi.org/10.1016/j.cej.2024.158585.
[50] Wang Q, Ren S, Hu S, Li X, Wang K, He W. Thermal decomposition synthesis of CuO on TiO_2 NTs as promising photocatalysts for effective photoelectrocatalytic hydrogen evolution and pollutant removal. Environ Res 2025;268. https://doi.org/10.1016/j.envres.2025.120780.
[51] Mróz K, Łabuz P, Kobielusz M, Pacia M, Kollbek K, Jabłoński P, et al. Copper oxide thin films as components for heterojunction formation with TiO_2 for photocatalytic CO_2 reduction. Catal Today 2024;441. https://doi.org/10.1016/j.cattod.2024.114890.
[52] Lipińska W, Grochowska K, Ryl J, Karczewski J, Sawczak M, Coy E, et al. Coupling between the photoactivity and CO_2 adsorption on rapidly thermal hydrogenated vs. conventionally annealed copper oxides deposited on TiO_2 nanotubes. J Mater Sci 2024:16947–62. https://doi.org/10.1007/s10853-024-10223-4.
[53] Noothongkaew S, Phongsapatcharamon T. Numerical investigation on performance improvement of CuO/TiO_2 heterojunctions for applications in sunlight-driven photodetectors and photocatalysts. J Nanoparticle Res 2024;26:1–12. https://doi.org/10.1007/s11051-024-05940-5.
[54] Villachica-Llamosas JG, Ruiz-Aguirre A, Colón G, Peral J, Malato S. CuO–TiO_2 pilot-plant system performance for solar photocatalytic hydrogen production. Int J Hydrogen Energy 2024;51:1069–77. https://doi.org/10.1016/j.ijhydene.2023.07.149.
[55] Ullah F, Ghani U, Mohamed Saheed MS. A PN-type CuO@TiO_2 nanorods heterojunction for efficient PEC water splitting: DFT model and experimental investigation on the effect of calcination temperature. Int J Hydrogen Energy 2023;48:39866–84. https://doi.org/10.1016/j.ijhydene.2023.07.159.
[56] Li S, Song T, Zhou W, Wang Z, Ma Y. Modulation of active site environment in an embedded CuO_x@TiO_2 photocatalyst for enhanced hydrogen evolution and CO_2 reduction. Mol Catal 2023;550. https://doi.org/10.1016/j.mcat.2023.113553.
[57] Mahato D, Gurusamy T, Ramanujam K, Haridoss P, Thomas T. Unravelling the role of interface of CuO_x-TiO_2 hybrid metal oxide in enhancement of oxygen reduction reaction performance. Int J Hydrogen Energy 2022;47:34048–65. https://doi.org/10.1016/j.ijhydene.2022.08.016.
[58] Baran Aydın E, Ateş S, Sığırcık G. CuO-TiO_2 nanostructures prepared by chemical and electrochemical methods as photo electrode for hydrogen production. Int J Hydrogen Energy 2022;47:6519–34. https://doi.org/10.1016/j.ijhydene.2021.12.032.